A New Optical Evaluation Approach for Parabolic Trough Collectors: First-Principle OPTical Intercept Calculation

Guangdong Zhu
Engineer IV
e-mail: Guangdong.Zhu@nrel.gov

Allan Lewandowski

National Renewable Energy Laboratory,
MS 5202, 15013 Denver West Parkway,
Golden, CO 80401

A new analytical method—First-principle OPTical Intercept Calculation (FirstOPTIC)—is presented here for optical evaluation of trough collectors. It employs first-principle optical treatment of collector optical error sources and derives analytical mathematical formulae to calculate the intercept factor of a trough collector. A suite of MATLAB *code is developed for FirstOPTIC and validated against theoretical/numerical solutions and ray-tracing results. It is shown that FirstOPTIC can provide fast and accurate calculation of intercept factors of trough collectors. The method makes it possible to carry out fast evaluation of trough collectors for design purposes. The FirstOPTIC techniques and analysis may be naturally extended to other types of CSP technologies such as linear-Fresnel collectors and central-receiver towers.* [DOI: 10.1115/1.4006963]

Keywords: parabolic trough, concentrating solar power, optical performance, optical analysis, intercept factor

1 Introduction

Parabolic trough collectors are one of the main concentrating solar power (CSP) technologies used in commercial utility-scale power generation plants [1]. As a means to collect solar energy, the optical performance is always viewed as one key technical aspect of parabolic trough collectors. This has a direct influence on annual electricity generation, annual plant revenue and, eventually, the levelized cost of energy (LCOE). The factors determining a trough collector's optical performance include the sun shape, various system optical/geometrical errors, and physical properties of system components. The sun shape originates from the finite size of the sun and is effectively broadened or altered by system errors such as reflector specularity, mirror slope error, receiver position error, and collector tracking error. An additional performance loss for a trough collector also comes from nonperfect material performance such as mirror reflectance, receiver surface absorption, and if applied, transmittance of receiver glass envelope [2].

One way to evaluate the optical performance of a trough collector is using the simplified beam spread method proposed by Bendt et al. [3]. This method uses a resulting beam spread distribution to represent the sun shape and all system optical errors. Each system optical error is approximated by a Gaussian-type probability function and convolved with the sun shape to formulate an effective beam cone. It then combines the beam spread distribution and receiver's angular acceptance function to calculate the intercept factor. The beam spread method is easy to use, but its approximation to actual system optical performance may not be sufficient for any analysis except for preliminary design.

A more accurate and commonly used approach is ray-tracing. Available ray-tracing software includes SOLTRACE [4], CIRCE [5,6], HELIOS [7], ENERTRACER [8], STARL [9], and some general-purpose optical analysis software like ASAP [10]. Ray-tracing generates a set of sun rays simulating the original or broadened/altered sun shape and lets them interact with various collector components with specified optical and mechanical properties for system components. The number of sun rays needs to be large enough to produce results with desired precision, and the computation, in some cases involving complex geometries and/or a large volume of data, can be time-consuming.

This paper presents a new analytical approach to assess the optical performance of a trough collector at normal incidence: First-principle OPTical Intercept Calculation (FirstOPTIC). FirstOPTIC applies the first-principle treatment to optical error sources for a trough collector through an analytical approach. By using the first-principle here, the authors understand that optical error sources are treated in the way they are typically characterized in laboratory measurements using a geometrical or optical interpretation [2]. For instance, slope error is measured as a geometrical deviation of actual mirror slope from desired values so it should be treated as a geometrical factor as a function of spatial variables [11–13], instead of a simple optical error distribution uniformly used for every point on the mirror surface. The latter will result in the loss of spatial dependence in slope error distribution and leads to inaccuracy of optical evaluation. The first-principle is used here to differentiate FirstOPTIC from the simple error-convolution approach often used by the Bendt et al. method in order to analytically evaluate the optical performance of a trough collector by characterizing optical errors in the way they are measured in a more fundamentally correct method.

The paper is organized as follows. General background information on parabolic trough collectors is given in Sec. 2; in Sec. 3, the methodology of FirstOPTIC is described in detail; Sec. 4 elaborates on the development and validation of the numerical code; Sec. 5 presents case study work to demonstrate FirstOPTIC's capability; and finally, the work in this paper is concluded in Sec. 6 along with future directions.

2 Background

Parabolic trough collectors can be described by two main characteristics: geometry and optics. Commercial trough collectors [14–16] often differ in either their specific geometry or optics, but they share the same general geometric and optical attributes.

Contributed by the Solar Energy Division of ASME for publication in the JOURNAL OF SOLAR ENERGY ENGINEERING. Manuscript received December 2, 2011; final manuscript received June 5, 2012; published online July 5, 2012. Assoc. Editor: Akiba Segal.

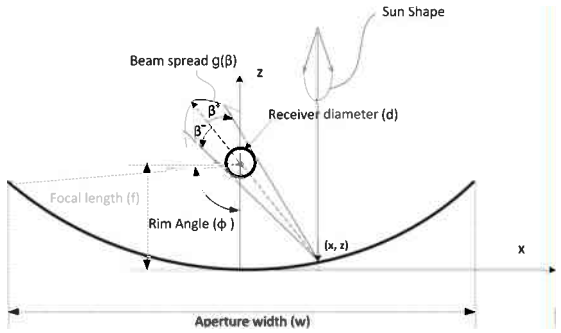

Fig. 1 Simplified representation of a trough collector. Note that the receiver size is exaggerated for demonstration purposes.

2.1 Collector Geometrical Representation. Figure 1 illustrates a simplified trough collector in two dimensions, which includes a parabola-shaped reflector and a receiver. The collector aperture width (w), focal length (f), receiver diameter (d), and the rim angle (ϕ) are labeled in the figure. The rim angle is usually less than 90 deg for practical applications. Receiver acceptance angle window (with the upper limit β^+ and the lower limit β^-) is also often used in the optical analysis and is defined as the angular range of beam spread distribution within which the sun rays would be intercepted by the receiver. The concentration ratio (C) is defined as the ratio of collector aperture width to the receiver circumference.

2.2 Collector Optical Interpretation. Both the optical properties and the mechanical precisions of the collector components affect the optical performance of a collector; these include mirror specularity, mirror slope error, receiver position error, and collector tracking error. Mirror surface imperfection is typically classified in two categories: mirror specularity and mirror slope error. Mirror specularity characterizes the imperfect surface microscopic texture of the reflective medium layer, while mirror slope error represents the deviation of mirror surface from its desired shape on medium and large scales due to the support structure and the substrate. Receiver position error may come from imperfect receiver support structure design, receiver sagging due to the weight of carried fluids and receiver itself, and the degradation of the collector structure over time. Collector tracking error defines the limitation of the tracking mechanism used by a collector.

The treatment of the sun shape and all error sources varies depending on the specific needs of the system optical characterization. In general, there are two approaches: first-principle and probability approximation.

2.2.1 First-Principle Approach. The sun shape is a brightness distribution of the sun disk and varies depending on the measurement location, the sky condition, the sun position, and many other relevant factors [2]. Its measurement may be expressed as the brightness as a function of angular variable. The vector emitting from the sun center to the earth is referred to as zero angle, i.e., the nominal direction. The measured brightness distributions do not approach a Gaussian [2,17]. The mirror specularity is the intensity distribution of the reflected beam and varies with light wavelengths and incidence angles. Due to the measurement difficulties [2,18,19], a probability distribution function is traditionally used to represent the widening effect of the specular reflection. The tracking error is the angular offset of a collector away from the sun position in the transversal plane and is mathematically equivalent to imposing the same angular offset to the originating beam relative to the receiver for a trough collector. The overall tracking error incorporating temporal effect can then be accounted precisely as a probability distribution by direct convolution with the originating beam. Again, this probability distribution is typically not a Gaussian.

Thus, starting from the first principles or equivalent to the first-principle treatment, the sun shape, the mirror specularity error, and the tracking error can be represented by a probability distribution function

$$E_{\text{source}\,i} = g_i(\beta) \tag{1}$$

which can take on almost any form (e.g., Gaussian, pillbox, delta, etc.). Here, β is the angular value measured from the nominal direction and i stands for each specific error source.

Mirror slope error and receiver position error are essentially the geometrical modification to the reflector surface and the receiver position, respectively. Mirror slope error is typically measured as angular deviation of the actual surface normal vector from the ideal as a function of spatial variables on a reflector surface. Its measurement often requires very sophisticated instrumentation [11–13]. The measured data set may include a large volume of data points, and its direct implementation as geometrical modifications could be very challenging. Receiver position error is the spatial deviation of receiver position from the focal point for a trough collector; it may vary along the receiver length for a single trough module and across a large number of collector modules for a utility-scale solar plant. Depending on the analysis purpose, the data set of the receiver position error may include one or a few data points for a module or a large volume of data points at a statistical level for a solar plant.

Starting from the first principles, both mirror slope error and receiver position error should be treated as the geometrical factors of a collector's optical performance, and equivalent mathematical formulae do not exist to directly convert them into a probability distribution, whereas this can be done for tracking error.

2.2.2 Probability-Approximation Approach. Mirror slope error and receiver position error may also be approximated by a probability distribution with some sacrifice in accuracy. For mirror slope error, an angular deviation of the surface normal vector at a point on the reflector results in twice the angular deviation of the reflected beam; thus, the probability approximation could directly use the probability distribution of the actual measurement data set. When the probability approximation is used, the spatial dependence of slope error would be lost: the overall slope error distribution is used at any point of the reflector instead of the local slope error at this point.

For receiver position error, there is no established relationship between the actual measurement data set and the probability distribution that can be used for direct convolution with the sun shape and other error sources. Very often, a simple Gaussian used in the analysis is typically based on empirical judgments.

Equation (1) can also be used to represent both mirror slope error and receiver position error as probability approximations. Then, an effective error cone can be obtained by convolving all error distributions and the sun shape to formulate the overall beam spread. The overall beam spread accounts for the sun shape and all system optical errors and may be represented by the following:

$$B_{\text{total}} = g_{\text{total}}(\beta) \tag{2}$$

Assuming the sun shape and all optical sources are a simple Gaussian as suggested by Bendt et al. [3], the convolution process can be simplified by using the mean value and root mean square (RMS) of Gaussian distribution functions. The mean value (μ_{total}) and RMS (σ_{total}) of the overall beam spread function (Eq. (2)) can be computed as follows:

$$\mu_{\text{total}} = \mu_{\text{sun}} + \mu_{\text{specularity}} + 2 \times \mu_{\text{slope}} + \mu_{\text{receiver}} + \mu_{\text{track}} \tag{3}$$

$$\sigma^2_{\text{total}} = \sigma^2_{\text{sun}} + \sigma^2_{\text{specularity}} + 4 \times \sigma^2_{\text{slope}} + \sigma^2_{\text{receiver}} + \sigma^2_{\text{track}} \tag{4}$$

Though the Bendt et al. approach has been widely used, it suffers from inaccurate evaluation of a collector's optical performance. First of all, the Bendt et al. approach loses spatial dependence of the mirror slope error and the receiver position error by using a probability approximation as a direct convolution with other error sources; second, by using a simple Gaussian, the Bendt et al. approach does not account for the systematic effects of the mirror slope error and the receiver position error. Very often, one needs to use ray-tracing software to more accurately assess a collector's optical performance. This paper proposes an alternative approach to treat the errors for trough collectors starting from the first principles.

One common parameter characterizing the collector optical performance is the intercept factor γ, which is defined as the ratio of solar power intercepted by the receiver to the solar power intercepted by the collector aperture. The optical efficiency can then be readily calculated as

$$\eta_{\text{optical}} = \gamma\rho\tau\alpha \tag{5}$$

Here, ρ is the reflector reflectance; τ is the transmittance of the receiver glass envelope; α is the average absorptance of receiver surface. The overall efficiency of a trough collector includes heat losses, but this analysis does not address those.

3 Methodology

The FirstOPTIC code calculates the intercept factor of a trough collector by employing first-principle treatment of the system optical error sources. The probability approximation for the sun shape, reflector specularity, and tracking error has been proven appropriate and accurate for trough collector optical analysis: the sun shape and reflector specularity are traditionally represented by their brightness/specular distributions, and the effect of the tracking error can be accounted precisely by direct convolution with the originating beam through an equivalent mathematical conversion. For a trough collector, an effective beam spread function, including the sun shape, the mirror specularity, and the tracking error, can then be defined as a probability function

$$B_{\text{eff}} = g_{\text{eff}}(\beta) \tag{6}$$

Here

$$\int_{-\infty}^{+\infty} g_{\text{eff}}(\beta)d\beta = 1 \tag{7}$$

3.1 Receiver Acceptance Angles. The acceptance angles are a function of position along the reflector aperture and are plotted in Fig. 2(*a*), where the top and bottom lines correspond to the receiver acceptance angle upper limit and lower limit, respectively. In the figure, a LS2 collector geometry was used ($w = 5$ m, $f = 1.49$ m, $d = 0.07$ m) [20]. The acceptance angle window is larger at the center of the reflector due to the relative shorter distance from the reflector to the receiver. For a trough collector with an ideal parabolic reflector surface and a perfectly positioned receiver, they are

$$\beta^{+}(x) = \sin^{-1}\left\{\frac{d}{2\cdot f\left[1+\left(\frac{x}{2\cdot f}\right)^2\right]}\right\} \tag{8}$$

$$\beta^{-}(x) = -\sin^{-1}\left\{\frac{d}{2\cdot f\left[1+\left(\frac{x}{2\cdot f}\right)^2\right]}\right\} \tag{9}$$

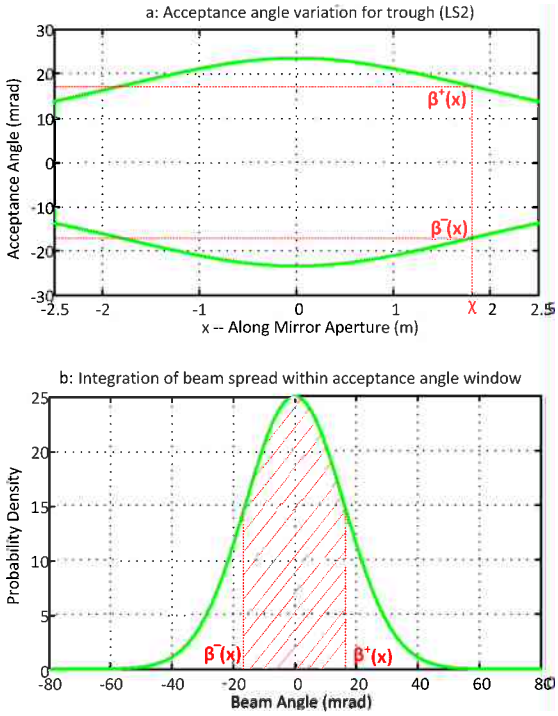

Fig. 2 Illustration of intercept factor calculation procedure

As shown in Fig. 2(*b*), the acceptance angles can then be used to calculate the local intercept factor through integration of probability density within the acceptance angle limits. Without considering mirror slope error and receiver position error, the calculation of acceptance angle limits is equivalent to the Bendt et al. approach [3].

3.2 First-Principle Treatment of Mirror Slope Error. Mirror slope error is the difference between the actual mirror slope and the ideal slope for a perfect parabolic surface. Inherently starting from the way the slope error is measured, it should be treated as part of the collector geometry. Figure 3 illustrates this geometrical effect. In part (*a*) of the figure, the mirror slope error changes the sun ray reflection directions, thus modifying the acceptance angle window for a receiver. It turns out that the impact to the receiver acceptance window is uniform across the collector aperture for a constant slope error. In Fig. 3(*b*), assuming a constant slope error of 3 mrad, the acceptance angle limits shift up by 6 mrad, indicated by the solid blue lines. The dashed lines are the acceptance angles for a perfect parabolic reflector and a perfectly positioned receiver, as given by Eqs. (8) and (9).

Mathematically, assume the mirror slope error to be

$$\epsilon_{\text{slope}} = \epsilon_{\text{slope}}(x) \tag{10}$$

Its impact on the receiver acceptance angles can then be represented as follows:

$$\beta^{+}_{\text{slope}}(x) = \beta^{+}(x) + 2 * \epsilon_{\text{slope}}(x) \tag{11}$$

$$\beta^{-}_{\text{slope}}(x) = \beta^{-}(x) + 2 * \epsilon_{\text{slope}}(x) \tag{12}$$

3.3 First-Principle Treatment of Receiver Position Error. When the receiver is misaligned from the focal point of a collector, the immediate consequence is a change in receiver acceptance angle. This is analogous to the impact of mirror slope error. Figure 4(*a*) illustrates the acceptance angles for a displaced receiver. The impact on the receiver acceptance angles varies

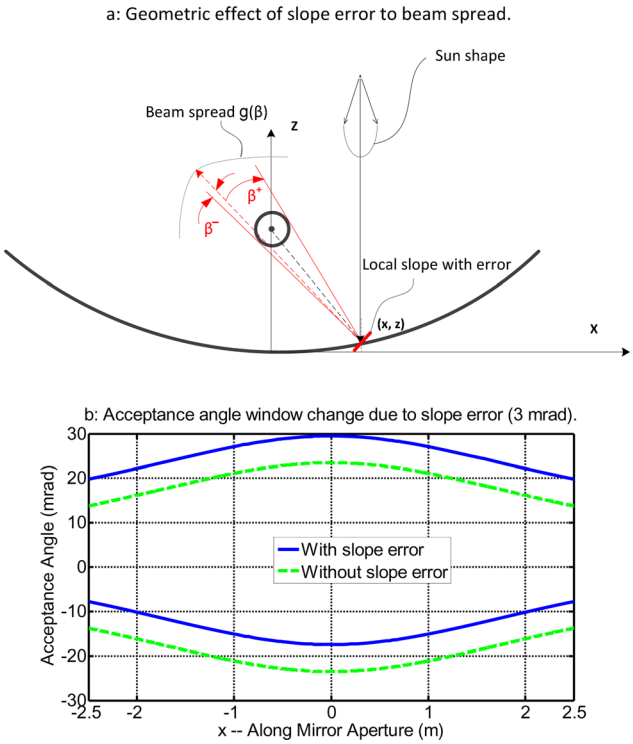

Fig. 3 Geometrical effect of mirror slope error

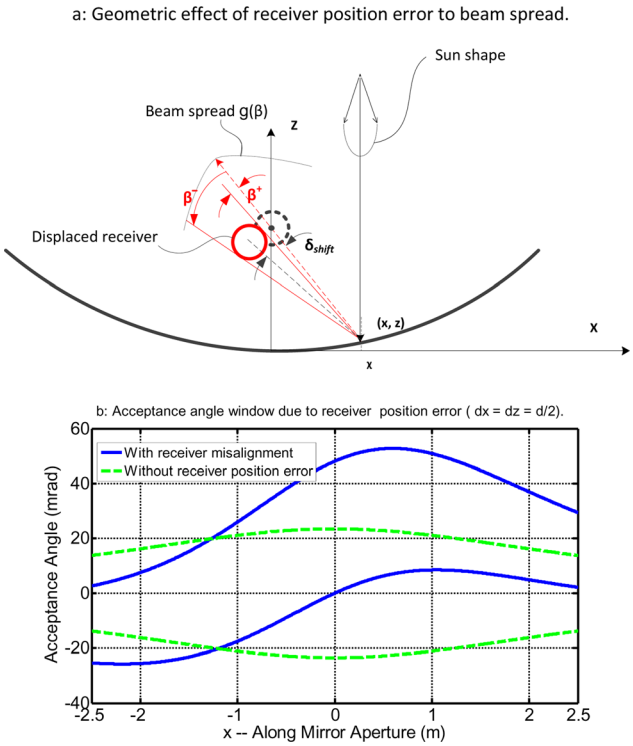

Fig. 4 Geometrical effect of receiver position error

across the collector aperture, as shown in Fig. 4(*b*). With receiver position error of only half a receiver diameter (35 mm) in both x and z for the LS2 collector, the receiver acceptance angles differ as much as roughly 30 mrad compared to a perfectly positioned receiver.

Assuming the receiver position error to be $(\Delta x, \Delta z)$, the receiver acceptance angles can be calculated as

$$\beta^{+}_{\text{receiver}}(x) = \delta_{\text{shift}}(x) + \sin^{-1}\left\{\frac{d}{2\cdot\sqrt{\left[(x-\Delta x)^2+\left(\frac{x^2}{4\cdot f}-f-\Delta z\right)^2\right]}}\right\} \tag{13}$$

$$\beta^{-}_{\text{receiver}}(x) = \delta_{\text{shift}}(x) - \sin^{-1}\left\{\frac{d}{2\cdot\sqrt{\left[(x-\Delta x)^2+\left(\frac{x^2}{4\cdot f}-f-\Delta z\right)^2\right]}}\right\} \tag{14}$$

Here, $\delta_{\text{shift}}(x)$ is the shifted angle for the receiver center due to position error and can be expressed in the vector's operation for convenience

$$\delta_{\text{shift}}(x) = \frac{(\overrightarrow{v_o}\times\overrightarrow{v_n})_y}{|(\overrightarrow{v_0}\times\overrightarrow{v_n})_y|}\cdot\cos^{-1}\left(\frac{\overrightarrow{v_0}\cdot\overrightarrow{v_n}}{|\overrightarrow{v_0}|\cdot|\overrightarrow{v_n}|}\right) \tag{15}$$

where $\overrightarrow{v_o}$ and $\overrightarrow{v_n}$ are the vectors from a point on the reflector surface to the collector focal point and the displaced receiver center, respectively

$$\overrightarrow{v_o} = \begin{pmatrix} x \\ 0 \\ z-f \end{pmatrix} \tag{16}$$

$$\overrightarrow{v_n} = \begin{pmatrix} x-\Delta x \\ 0 \\ z-f-\Delta z \end{pmatrix} \tag{17}$$

And (x, z) is a point on the parabolic reflector surface, i.e., $z = \frac{x^2}{4f}$.

3.4 Intercept Factor. With both mirror slope error and receiver position error present, the combined impact on receiver acceptance angles is additive

$$\beta^{+}_{\text{slope+receiver}}(x) = \beta^{+}(x) + 2*\epsilon_{\text{slope}}(x) + \left(\beta^{+}_{\text{receiver}}(x) - \beta^{+}(x)\right) \tag{18}$$

$$\beta^{-}_{\text{slope+receiver}}(x) = \beta^{-}(x) + 2*\epsilon_{\text{slope}}(x) + \left(\beta^{-}_{\text{receiver}}(x) - \beta^{-}(x)\right) \tag{19}$$

For a point x on a trough collector, the local intercept factor can be calculated as

$$\gamma(x)\int_{\beta^{-}_{\text{slope+receiver}}(x)}^{\beta^{+}_{\text{slope+receiver}}(x)} g_{\text{eff}}(\beta)d\beta \tag{20}$$

Integration of $\gamma(x)$ over the collector aperture yields the intercept factor

$$\gamma^0 = \frac{1}{w}\cdot\int_{-\frac{w}{2}}^{\frac{w}{2}}\gamma(x)dx \tag{21}$$

When the local intercept factor varies along collector length l, i.e., $\gamma = \gamma(x, y)$, the collector intercept factor becomes

Table 1 Test cases using the LS2 trough collector

Case \ Optics	Sun shape	Mirror specularity	Tracking error	Slope error	Receiver position error
I	Gaussian: $\sigma = 3$ mrad	Gaussian: $\sigma = 5$ mrad	Gaussian: $\sigma = 9.32$ mrad	None	None
II	CSR10 [17]	Gaussian: $\sigma = 8.88$ mrad	Gaussian: $\sigma = 6$ mrad	None	None
III	None	None	None	None	$\Delta x = -35$ mm; $\Delta z = -35$ mm
IV	None	None	None	Constant: 6.8 mrad	None
V	None	None	None	Measured data set in Fig. 5	None
VI	CSR10 [17]	Gaussian: $\sigma = 0.6$ mrad	Gaussian: $\sigma = 0.8$ mrad	Measured data set in Fig. 5	$\Delta x = -20$ mm; $\Delta z = 30$ mm

$$\gamma^0 = \frac{1}{w \cdot l} \cdot \int_{-\frac{1}{2}}^{\frac{1}{2}} \int_{-\frac{w}{2}}^{\frac{w}{2}} \gamma(x, y) dx dy \tag{22}$$

A similar geometrical treatment can also be applied to the tracking error. For parabolic trough collectors, it is mathematically equivalent to treat the tracking error as a probability approximation. However, this may not be the case for other types of collectors, such as linear Fresnel and central-receiver towers. When this occurs, the geometrical impact of the tracking error on the receiver acceptance angles needs to be derived as well.

3.5 Notes. FirstOPTIC shares some same concepts with the Bendt et al. probability-approximation approach, such as acceptance angle, but takes one more step to apply first-principle treatments to the system error sources; it is fundamentally equivalent to performing ray-tracing simulation for sun rays as a whole, instead of tracing each individual sun ray. The work in this paper focuses on intercept factor calculation for trough collectors at normal incidence angle, and the three-dimensional effects due to nonzero incidence angles will be addressed in future work.

4 Code Development

A suite of MATLAB code [21] has been developed for FirstOPTIC. In the code, the sun shape, mirror specularity, and tracking error can be defined as either a non-Gaussian distribution or a simple Gaussian. The code applies geometrical treatments to slope error and receiver position error in either one or two dimensions. To validate the developed code and test its capability, a series of test cases were generated by using the LS2 collector geometry, as in Table 1. For mathematical simplicity, zero mean values were assumed for all errors given by a Gaussian distribution. SOLTRACE [4] is used to provide ray-tracing results for all test cases. SOLTRACE is a Monte-Carlo ray-tracing tool developed for solar concentrator applications. It has been proven to provide accurate optical evaluation for a variety of solar concentrating applications [4].

The cases in Table 1 are selected only for validation purposes (i.e., they are not intended to represent real situations) and are designed in a way to separate all optical errors for individual validation. A tremendous effort was taken to design cases with available theoretical/numerical solutions for comparison when the difference between FirstOPTIC and SOLTRACE arises. For case I where all optical errors represented by a probability distribution are a simple Gaussian and there is no mirror slope error or receiver position error, a numerical solution can be readily derived according to Bendt et al. [3]. Cases II and VI use the CSR10 sun shape data measured by Neumann et al. [17]. For case III where only the receiver position error is present, the intercept factor will be 0.5 when the position offset is exactly half of the receiver diameter along x and z.

When only the slope error is specified (i.e., no other errors are present), the intercept factor can be calculated through a simple numerical scheme. First, examine the acceptance angles for each individual point on the reflector surface against its local slope error, noting the fact that the impact of a constant slope on the acceptance angle is uniform through the collector aperture (whereas its impact on the intercept factor is not). Whether a reflected sun ray will miss the receiver can be determined immediately by comparing local slope error with the local receiver acceptance angle window. The smallest acceptance angle for a LS2 collector is about 13.79 mrad at the rim. According to Eqs. (11) and (12), a constant slope error of 6.8 mrad in case IV would give at most 13.6 mrad derivation for a reflected sun ray from its nominal direction, and all rays should hit the receiver when assuming zero errors for all other system error sources and a point-source sun. Thus, the intercept factor should be 1 for case IV. A similar calculation can be applied to case V and used to derive the corresponding intercept factor. For case V, a set of measured slope error data for a LS2 collector is used, as plotted in Fig. 5. In the figure, the y axis represents the length of the collector. The slope error is measured for a full LS2 module. Part (a) of Fig. 5 shows a color-scaled map of slope error, and part (b) provides a probability distribution of this measurement data set. It is clearly shown that the slope error results from a certain type of systematic effect and is obviously not a simple Gaussian.

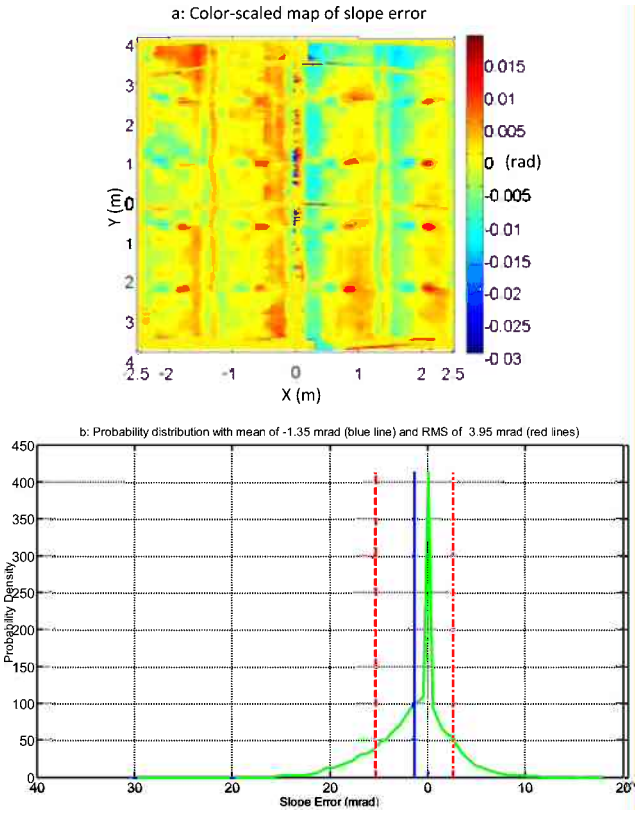

Fig. 5 A set of measured mirror slope error ($\partial z/\partial x$ only)

Table 2 Comparison of results for the intercept factor using various methods. Here, superscript T means theoretical solution; superscript N means numerical solution.

Methods \ Case	I	II	III	IV	V	VI
Theoretical/ numerical	$0.9126^{\text{N-Bendt}}$	N/A	0.5^{T}	1^{T}	0.967^{N}	N/A
FirstOPTIC	0.9126	0.9063	0.5001	1.0000	0.9673	0.7081
SOLTRACE	0.9200	0.9162	0.5001	0.9872	0.9723	0.7320

A comparison of the results is summarized in Table 2. The theoretical/numerical solutions are provided when available. The results for FirstOPTIC are calculated using spatial resolution of 1001 points along the collector aperture, and the results for SOLTRACE are based on $1–5 \times 10^6$ sun rays depending on the limit of memory usage for each case. For FirstOPTIC and theoretical/numerical predictions, there exists nearly perfect agreement. The results between FirstOPTIC and SOLTRACE match well in general but show a slightly larger difference for cases IV, V, and VI. Since FirstOPTIC agrees better with the theoretical/numerical solutions than SOLTRACE does, it is fair to conclude that FirstOPTIC provides more accurate results than SOLTRACE.

After further investigation, it is found that the differences between FirstOPTIC and SOLTRACE do not solely result from the limited number of sun rays used by SOLTRACE. For cases IV, V, and VI, the collector surface was defined by a set of discrete points (350,000) as shown in Fig. 5, and the overall surface needs to be geometrically reconstructed through a surface interpolation. The surface normal vector of the reconstructed surface would sustain a numerical error proportional to the local surface slope (in the order of radians), which may then be comparable to the slope error (in the order of a few milliradians). It is the surface interpolation scheme that gives rise to the slightly larger errors in the results for SOLTRACE. The surface interpolation scheme in a three-dimensional space is always a challenging issue in many related areas [22], such as fluid mechanics and structural analysis. It has been planned to develop a more accurate surface interpolation scheme for SOLTRACE in the future. In comparison, a set of discrete data points can be directly used for the optical evaluation in FirstOPTIC, and the surface reconstruction is not required.

The required computational efforts of FirstOPTIC and SOLTRACE are also examined and plotted in a log scale as a function of relative error against the theoretical/numerical results for cases III and V, as shown in Fig. 6. All simulations were carried out using one CPU on a Dell computer with Intel Core i7 CPU of 2.67 GHz and a RAM of 1.17 GHz and 3.24 GB. The relative error decreases with increasing numerical resolution for FirstOPTIC or increasing number of sun rays for SOLTRACE. Each case involves 350,000 data points for the reflector surface. The largest number of sun rays used for SOLTRACE is 5×10^6 for case III and 1×10^6 for case V due to a memory issue. For each case, the computational time for SOLTRACE is significantly longer than that of FirstOPTIC: it was 0.016 s for FirstOPTIC and 0.72 s for SOLTRACE when reaching a precision of 0.25% for case III (FirstOPTIC is 45 times faster); as for case V, it took FirstOPTIC 0.078 s to achieve a precision of 0.29% while it took SOLTRACE about 71,400 s to achieve a precision of 0.42% (FirstOPTIC is over 900,000 times faster!). In addition, the FirstOPTIC code requires much less computer memory than SOLTRACE, and it can much more conveniently achieve very high precision. SOLTRACE encountered a memory issue when more than 1×10^6 sun rays were used for case V (note that 350,000 points were used for the reflector surface).

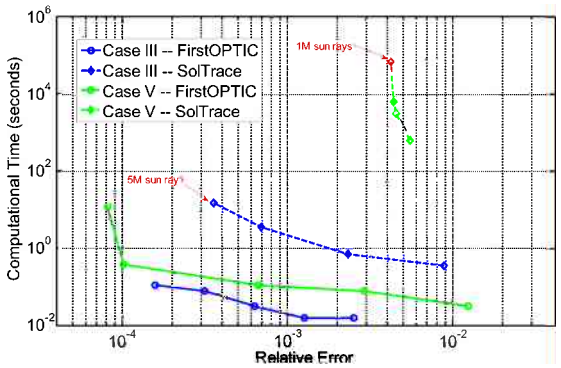

Fig. 6 Comparison of computational time between FirstOPTIC and SOLTRACE

For the cases involving or not involving a large number of discrete surface points, FirstOPTIC exhibits substantial advantages in computational accuracy and speed compared to SOLTRACE. This largely comes from the analytical nature of FirstOPTIC. The FirstOPTIC code does not have to generate a large number of sun rays, trace each sun ray vector, and calculate its potential interactions with other surfaces, as SOLTRACE or other ray-tracing programs do. Instead, it treats the sun ray beam as a whole and calculates the angular range of the sun ray beam intercepted by the receiver. However, FirstOPTIC does not calculate the receiver surface absorptance of sun rays as a function of incidence angle; it also does not calculate the flux map on the receiver surface as a ray-tracing program can do. Overall, the newly developed FirstOPTIC code is a valuable tool when flux maps are not required for the analysis.

5 Case Study

After the validation of the FirstOPTIC code, a case study is performed to compare the difference between the first-principle approach and the probability-approximation approach for the receiver position error.

First, a procedure is developed to establish a corresponding probability distribution for an actual receiver position error because one did not previously exist. When the receiver is misaligned with a certain position error in both x and z directions, the receiver acceptance angle window will be changed. A reasonable probability approximation for its impact on the final beam spread distribution calculates the angular offset due to the receiver position error for points along the collector aperture and derives its probability distribution. This can then be convolved with other error distributions. Two examples are shown in Fig. 7. Parts (a) and (b) of the figure show the probability density as a function of angular beam offset resulting from receiver position error $\Delta x = 15$ mm and $\Delta z = 15$ mm, respectively. The blue solid vertical line labels the mean value of the distribution, and the dashed red lines label the standard deviation (i.e., RMS). Note that the distribution is very different from a Gaussian behavior. The probability-approximation approach convolves the actual non-Gaussian distribution with the sun shape and the rest of the system error distributions to obtain the overall beam spread. For the analysis in this section, a reference collector is used: the aperture width $w = 6$ m; the focal length $f = 1.71$ m; the receiver diameter $d = 0.08$ m [19]. The collector length is assumed to be 1. The sun shape is defined by the CSR10 measurement [17] and the slope error data are assumed to follow a Gaussian distribution with the RMS of $\sigma_{\text{slope}} = 2.5$ mrad, and the rest of the system errors are approximated by a Gaussian distribution for convenience, i.e., the RMS of the mirror specularity error $\sigma_{\text{specularity}} = 0.6$ mrad, the RMS of tracking error $\sigma_{\text{track}} = 1$ mrad.

Each plot in Fig. 8 compares the results by using the first-principle treatment (FirstOPTIC) and the probability approximation. It is observed that the larger the receiver position error in either x or z direction, the larger the discrepancy between two methods. For the 30 mm position error in x and z, the relative error of the intercept factor resulting from the probability

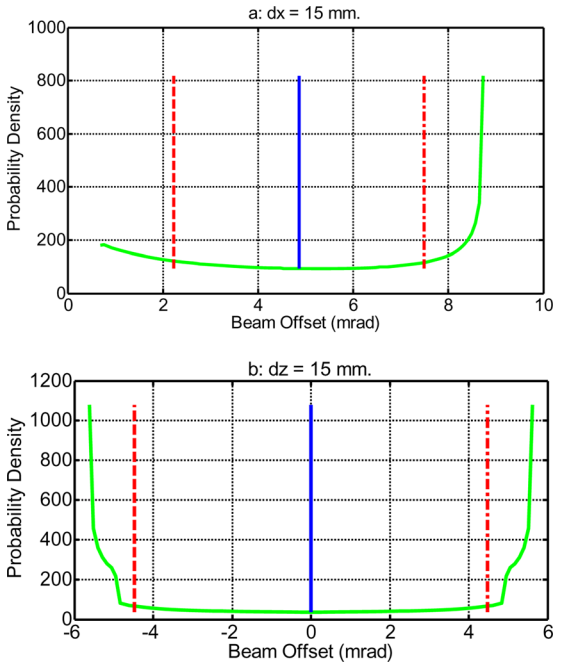

Fig. 7 Angular offset to the beam spread induced by receiver position errors. The solid vertical line marks the mean value, and the dashed vertical lines mark the RMS of the distribution.

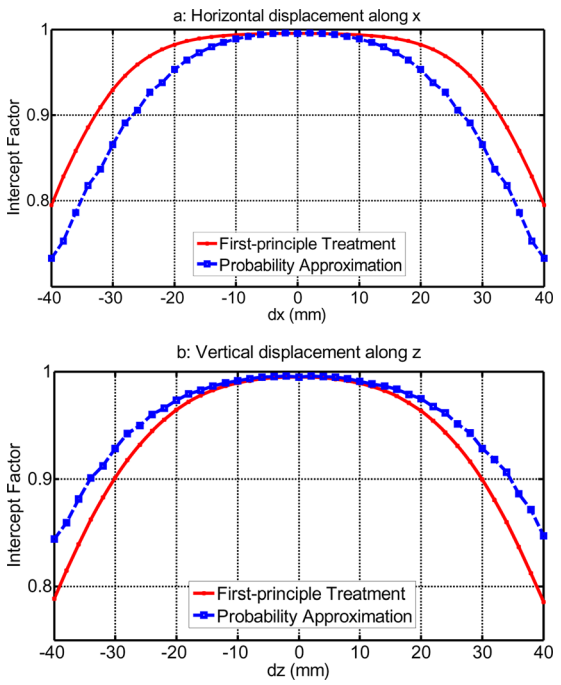

Fig. 8 Intercept factor as a function of receiver position error along *x* (*a*) and along *z* (*b*)

approximation is about 6.8% and 3.2%, respectively, compared with the first-principle treatment. It is also interesting to note that the probability-approximation approach underestimates the collector performance for position error in x while it overestimates for position error in z.

6 Conclusions

Optical performance of trough collectors is critical for trough collector designs and is often evaluated using either a simple but not accurate analytical probability-approximation method or an accurate but potentially time-consuming ray-tracing technique. The method proposed here—FirstOPTIC—provides a fast and accurate tool to evaluate the optical performance of trough collectors. The analytical nature of the method can make it suitable for fast evaluation of large sets of collector design options, while the first-principle treatment of optical error sources inherent in this method yields high accuracy for the results.

The FirstOPTIC code developed here is validated and used to investigate the accuracy of probability approximation of receiver position error. In the future, FirstOPTIC will be enhanced to take into account three-dimensional effects for trough collectors at nonzero incidence angle and is planned to be further extended to linear-Fresnel collectors and to central-receiver towers.

Acknowledgment

This work was supported by the U.S. Department of Energy under Contract No. DE-AC36-08GO28308 with the National Renewable Energy Laboratory (NREL). The authors would like to thank the thermal systems group staff at NREL for providing their valuable feedbacks for this work.

Nomenclature

γ = the collector intercept factor
ρ = the reflector reflectance of the reflector
τ = the transmittance of the receiver glass envelope
α = the absorptance of the receiver surface
η_{optical} = the collector optical efficiency
w = the collector aperture width, m
f = the reflector focal length, m
d = the receiver diameter, m
φ = the collector rim angle, rad
C = the collector concentration ratio
β = the angular variable
x = the coordinate along collector aperture, m or mm
y = the coordinate along collector length, m or mm
z = the coordinate along the normal vector of the collector aperture, m or mm
Δx = the receiver position error along x direction, mm
Δz = the receiver position error along z direction, mm
β^+ = the upper limit of the receiver acceptance angle window, mrad
β^- = the lower limit of the receiver acceptance angle window, mrad
β^+_{slope} = the upper limit of the receiver acceptance angle window with the reflector slope error, mrad
β^-_{slope} = the lower limit of the receiver acceptance angle window with the reflector slope error, mrad
$\beta^+_{\text{receiver}}$ = the upper limit of the receiver acceptance angle window with the receiver position error, mrad
$\beta^-_{\text{receiver}}$ = the lower limit of the receiver acceptance angle window with the receiver position error, mrad
$\beta^+_{\text{slope+receiver}}$ = the upper limit of the receiver acceptance angle window with the reflector slope error and receiver position error, mrad
$\beta^-_{\text{slope+receiver}}$ = the lower limit of the receiver acceptance angle window with the reflector slope error and the receiver position error, mrad
i = an index

$E_{\text{source } i}$ = the distribution function for a collector optical error source i
g = a general distribution function
g_{eff} = the effective beam spread distribution
μ = the mean value of a distribution
σ = the root mean square of a distribution
μ_{total}, σ_{total} = the mean value and the root mean square of the overall beam spread function, mrad
μ_{sun}, σ_{sun} = the mean value and the root mean square of the sun shape distribution, mrad
$\mu_{\text{specularity}}$, $\sigma_{\text{specularity}}$ = the mean value and the root mean square of the reflector specularity distribution, mrad
μ_{slope}, σ_{slope} = the mean value and the root mean square of the reflector slope error distribution, mrad
μ_{receiver}, σ_{receiver} = the mean value and the root mean square of the receiver position error distribution, mrad
μ_{track}, σ_{track} = the mean value and the root mean square of the collector tracking error distribution, mrad
ϵ_{slope} = the reflector slope error at a point, mrad
∂ = the partial differential operator

References

[1] Kearney, D., and Morse, F., 2010, "Bold, Decisive Times for Concentrating Solar Power," Sol. Today, **24**(4), pp. 32–35.
[2] Rabl, A., 1985, *Active Solar Collectors and Their Applications*, Oxford University Press, New York.
[3] Bendt, P., Rabl, A., Gaul, H. W., and Reed, K. A., 1979, "Optical Analysis and Optimization of Line Focus Solar Collectors," Paper No. SERI/TR-34-092, SERI, Golden, CO.
[4] Wendelin, T., 2003, "SOLTRACE: A New Optical Modeling Tool for Concentrating Solar Optics," 2003 International Solar Energy Conference, Hawaii.
[5] Ratzel, A. C., and Boughton;, B. D., 1987, "CIRCE.001: A Computer Code for Anaysis of Point-Focus Concentrators With Flat Targets," Paper No. SAND86-1866, Sandia National Laboratories, Albuquerque, NM.
[6] Romero, V. J., 1994, "CIRCE2/DEKGEN2: A Software Package for Facilitated Optical Analysis of 3-D Distributed Solar Energy Concentrators—Theory and User Manual," Sandia National Laboratories, Albuquerque, NM.
[7] Biggs, N., and Vittitoe, C. N., 1976, "The Helios Model for the Optical Behavior of Reflecting Solar Concentrators," Sandia National Laboratories, Albuquerque, NM.
[8] Blanco, M., and Alarcon, D., 2000, "ENERTRACER: A New Computer Tool for Energy Concentrating Systems," Proceedings of the Solar Thermal 2000 Renewable Energy for the New Millennium Conference, Sydney, Australia, pp. 87–93.
[9] Belhomme, B., Pitz-Paal, R., Schwarzbozl, P., and Ulmer, S., 2009, "A New Fast Ray Tracing Tool for High-Precision Simulation of Heliostat Fields," J. Sol. Energy Eng., **131**(8), 031002.
[10] "ASAP," 2012, Breault Research Organization, http://www.breault.com/software/asap.php
[11] Wendelin, T., May, K., and Gee, R., 2006, "Video Scanning Hartmann Optical Testing of State-of-the-Art Parabolic Trough Concentrators," Solar 2006 Conference, Denver, CO.
[12] Andraka, C., Sadlon, S., Myer, B., Trapeznikov, K., and Liebner, C., 2009, "SOFAST: Sandia Optical Fringe Analysis Slope Tool for Mirror Characterization," SolarPACES 2009, Berlin, Germany.
[13] Pottler, K., Lupfert, E., Johnston, G., and Shortis, M., 2005, "Photogrammetry: A Powerful Tool for Geometric Analysis of Solar Concentrators and Their Components," J. Sol. Energy Eng., **127**(1), pp. 94–101.
[14] Price, H., Lupfert, E., Kearney, D., Zarza, E., Cohen, G., Gee, R., and Mahoney, R., 2002, "Advances in Parabolic Trough Solar Power Technology," J. Sol. Energy Eng., **124**(2), pp. 109–125.
[15] Riffelmann, K.-J., Graf, D., and Nava, P., 2011, "Ultimate Trough—The New Parabolic Trough Collector Generation for Large Scale Solar Thermal Power Plants," Proceedings of the ASME 2011 5th International Conference on Energy Sustainability, Washington, DC.
[16] Far, A., and Gee, R., 2009, "The SkyTrough Parabolic Trough Solar Collector," Proceedings of the ASME 2009 3rd International Conference of Energy Sustainability, San Francisco, CA.
[17] Neumann, A., Witzke, A., Jones, S. A., and Schmitt, G., 2002, "Representative Terrestrial Solar Brightness Profiles," J. Sol. Energy Eng., **124**, pp. 198–204.
[18] Meyen, S., Lupfert, E., Pernpeintner, J., and Fend, T., 2009, "Optical Characterization of Reflector Material for Concentrating Solar Power Technology," SolarPACES 2009, Berlin, Germany.
[19] Gee, R., Brost, R., Zhu, G., and Jorgensen, G., 2010, "An Improved Method for Characterizing Reflector Specularity for Parabolic Concentrators," SolarPACES 2010, Perpignan, France.
[20] Price, H., and Kearney, D., 2005, "Chapter 6: Recent Advances in Parabolic Trough Solar Power Plant Technology," NREL Report No. CH-550-36422.
[21] "MATLAB—The Language of Technical Computing," 2012, The MathWorks, Inc., Natick, MA, http://www.mathworks.com/products/matlab/index.html
[22] Zhu, G., Mammoli, A., and Power, H., 2006, "A 3-D Indirect Boundary Element Method for Bounded Creeping Flow of Drops," Engineering Analysis With Boundary Elements, Vol. 30, pp. 856–868.